Optical properties and first principles study of $CH_3NH_3PbBr_3$ perovskite structures for solar cell application

Asma O. Al Ghaithi [1], S. Assa Aravindh [2], Mohamed N. Hedhili [3], Tien Khee Ng [3], Boon S. Ooi [3], and Adel Najar [1,*]

[1] Department of Physics, College of Science, United Arab Emirates University, Al Ain 15551, UAE

adel.najar@uaeu.ac.ae

[2]Nano and Molecular Systems Research Unit, University of Oulu, P.O. Box 8000, FI-90014, Oulu, Finland

[3]King Abdullah University of Science and Technology (KAUST), Thuwal 23955-6900, Saudi Arabia

Abstract. Solution-processed organic–inorganic hybrid perovskites have attracted attention as light-harvesting materials for solar cells and photonic applications. The present study focusses on cubic single crystal; microstructures of $CH_3NH_3PbBr_3$ perovskite fabricated by a one-step solution based self-assembly method. It is seen that, in addition to the nucleation from the precursor solution, the crystallization occurs when the solution was supersaturated, followed by formation of small nucleus of $CH_3NH_3PbBr_3$ that will self-assembled into bigger hollow cubes. A 3D fluorescence microscope investigation of hollow cubes confirmed the formation of hollow plates on the bottom, then the growth starts from the perimeter and propagate to the center of the cube. Furthermore, the growth in the (001) direction follows a layer-by-layer growth model to form a complete cube, confirmed by SEM observations. To get more insights into the structural and optical properties, density functional theory (DFT) simulations were conducted. The density of state (DOS) calculations revealed that the valence band maximum (VBM) consists of states contributed by Br and Pb, which agrees with the X-ray photoelectron spectroscopy valence band (XPSVB) measurements.

Keywords: Perovskite, Optical materials, DFT.

1 Introduction

Organic-inorganic perovskites in the form of thin films, microcrystals, nanoparticles and bulk single-crystals exhibit outstanding optoelectronic properties [1]. They are attractive candidates in many cutting-edge applications such as solar cells, light-emitting diodes (LEDs), lasers, and photodetectors [2-6] and a competitive material to many standard semiconductors [7-12]. The properties of perovskites depend highly on the composition, crystallinity and its morphology. They belong to a large crystallo-

graphic family that adopt the same crystal structure as calcium titanate (CaTiO3) [13, 14], and has the general ABX3, three-dimensional (3D) structural framework [15], where A and B are cations of different sizes and X is an anion [16]. Different preparation of perovskite nanostructures: thin film for solar cells [17], 2D nanoplates [18], 1D nanowires [19], and quantum dots [20] have been studied at the microscale and nanoscale levels. Also, the trap-state density and carrier diffusion length have been investigated in bulk perovskite single crystal [21]. However, low-dimensional halide perovskites show optical and electrical properties that are different from bulk halide perovskites [22]. Hence the control of the scale and the shape of the synthesized perovskite are necessary for fundamental and applications research. The changes in optical and electrical properties are attributed to the quantum size effects, large surface-to-volume ratio, and anisotropic geometry [23]. Several synthesis methods were used to prepare single crystal $CH_3NH_3Pb\mathit{X}_3$, such as top-seed solution growth [24], inverse temperature crystallization [25, 26], and anti-solvent vapor-assisted crystallization [27]. Recently, researchers were interested in the nucleation and growth mechanisms of perovskite structures prepared by inverse temperature crystallization method, using grazing incidence X-ray diffraction or in situ Fourier transform infrared spectroscopy. These techniques can accurately explain the crystallinity of the material and its chemical composition [28]. For example, F. Chen et al. have used filter paper inserted between substrate and precursor solution droplet to separate $CH_3NH_3PbBr_3$ from DMF solution, and followed by the crystallization mechanisms [29]. However, not many studies were conducted focusing on the detailed growth mechanism of cubic $CH_3NH_3PbBr_3$, evolution of its morphology, and optical properties followed by in-depth analysis using first principles methods.

In this work, $CH_3NH_3PbBr_3$ microstructures were synthesized using a one-step solution self-assembly method. The morphology and the structure were analyzed using SEM, and X-ray diffraction. Scanning electron microscopy (SEM) and 3D fluorescence microscope observations were used to explain the growth mechanism. We also carried out first principles based density functional theory (DFT) simulations to explain the electronic properties of cubic $CH_3NH_3PbBr_3$ microstructures.

2. Experimental methods

2.1 Synthesis of hybrid organic-inorganic perovskite $CH_3NH_3PbBr_3$

The hybrid organic-inorganic perovskite under this study is $CH_3NH_3PbBr_3$. The $CH_3NH_3PbBr_3$ microstructures (hollow cubes, plates, cubes, and wires) were synthesized using a one-step solution self-assembly method, which has been reported in Ref. [30-32]. CH_3NH_3Br and $PbBr_2$ were independently dissolved in N-N-dimethylformamide (DMF) with the same concentration equal to 0.2 M. These two solutions were mixed at room temperature with 1:1 volume ratio to form CH_3NH_3Br - $PbBr_2$ solution with concentration equal to 0.1 M. The diluted solution was dip-casted onto a glass or silicon substrate, which was placed on a Teflon stage in a beaker. Dichlorometane (DCM) of CH_2Cl_2 was placed in the beaker and sealed with a porous

Parafilm to control the evaporation speed. After 24 hours, $CH_3NH_3PbBr_3$ perovskites microstructures were successfully synthesized on the silicon substrate.

2.2 Physical characterization and Computational methodology

The fabricated structures were then characterized using SEM, and X-ray powder diffraction to study its morphology and crystallinity. Scanning electron microscopy (SEM) Jeol operating at 20 keV beam energy was used to analyses the structures. X-ray photoelectron spectroscopy (XPS) studies were carried out in a Kratos Axis Supra DLD spectrometer equipped with a monochromatic Al Kα X-ray source (hν = 1486.6 eV) operating at 45 W, a multi-channel plate and delay line detector under a vacuum of ~10-9 mbar. All spectra were recorded using an aperture slot of 300 μm x 700 μm. Survey spectra were collected using a pass energy of 160 eV and a step size of 1 eV. A pass energy of 20 eV and a step size of 0.1 eV were used for the high-resolution spectra. For XPS analysis samples were mounted in floating mode to avoid differential charging. Charge neutralization was required for all samples. Binding energies were referenced to the C 1s binding energy of adventitious carbon contamination which was taken to be 284.8 eV. We have carried out density functional theory calculations on bulk $CH_3NH_3PbBr_3$ to get further insight into the experimentally observed properties employing the plane wave pseudopotential code, Vienna Abinitio Simulation Package (VASP) [33, 34]. The exchange and correlation are described in the generalized gradient approximation (GGA) [35]. The pseudopotentials were described in the projected augmented wave (PAW) method with Perdew-Burke-Ernzerhof (PBE) formalism [36]. A kinetic energy cut-off of 650 eV is used to expand the plane waves included in the basis set. Since it is well known that GGA underestimates the bandgap of halide perovskite structures, [37], we have employed the Hubbard approximation with U parameter = 8eV [38] as implemented in the Dudarev approach in VASP. The Brillouin zone is sampled using a Monkhorst Pack grid of 8×8×8. The energy and force relaxations were performed within tolerances of 1E-06 eV and 1E-03 eV/Å respectively.

3 Results and discussions

The scanning electronic microscopy (SEM) observations of $CH_3NH_3PbBr_3$ structures shows a wide range of shapes; cubes, plates, wires and hallow cubes (Figure 1(a)) formed on silicon substrate. The range of wires in length is from few microns to more than 100 μm and in width from few hundred nm to 40 μm. Most of wires were found to have rectangular cross-sections as shown in Figure 1(a)-(b). A cubes and plates with sharp edges are existing with different sizes. Also, hollow cubes appeared with sharp edge (see Figure 1(c)). These hollow cubes are in the early crystallization stages due to the formation of agglomerate crystals and it seems that the growth starts from the perimeter and propagate to the center of the cube [39].

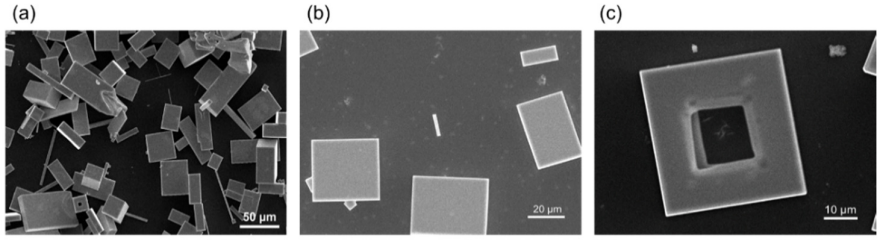

Fig. 1. (a) SEM images of $CH_3NH_3PbBr_3$ perovskite structures: (b) plates and (c) hollow cubes.

To explain the growth mechanism through surface evolution, several plates, cubes, and hollow cubes were observed using 2D and 3D florescence microscope coupled with SEM observations. The schematic representation in Figure 2(a), present an approach of growth and crystallization mechanisms of $CH_3NH_3PbBr_3$ structures.

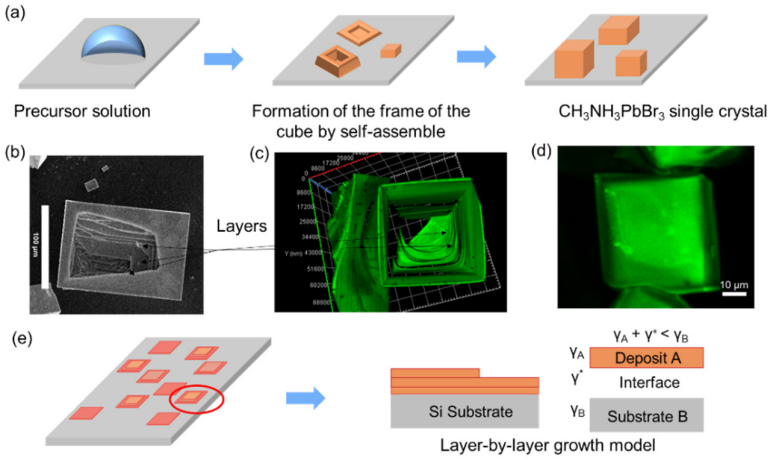

Fig. 2. (a) Schematic scenario of growth process of $CH_3NH_3PbBr_3$ microstructures. (b)-(c) SEM and 3D fluorescence microscope images of perovskite showing hollowed interior. (d) 2D fluorescence microscope images of $CH_3NH_3PbBr_3$ plates. (e) Schematic representation of a layer-by-layer (Frank–Van der Merwe) growth model of $CH_3NH_3PbBr_3$ single crystal in (001) direction.

The growth starts when the crystallization occurs in the supersaturated CH_3NH_3Br•PbBr2•DMF precursor solution, and $CH_3NH_3PbBr_3$ molecules condense into small seeds. These CH3NH3PbBr3 seeds coalesce into bigger particles after short time. Then, $CH_3NH_3PbBr_3$ particles gradually self-assembled into a hollow structure like hollow cage and the growth starts from the perimeter and propagate to the center (see Figure 1b), giving forms of hollow cubes when the growth is not finished due to the lack in the crystal. These crystals are twisted and their faces peculiarly inclined

toward each other. A 3D fluorescence microscope and SEM observations confirm the presence of hollow cubes in Figure 3b-c with formation of hollow plate in the bottom and then $CH_3NH_3PbBr_3$ crystals accumulate in layered stacked structure, and continued to grow in (001) direction until the final cubic single crystal is formed. Indeed, the growth of $CH_3NH_3PbBr_3$ crystals in (001) direction was done by layer-by-layer model also known as the Frank–van der Merwe growth mode till the formation of the complete cube. To explain the growth mechanism of these structures in (100) direction, a schematic scenario is represented in Figure 2(e). Small plates of $CH_3NH_3PbBr_3$ crystal appeared on the bottom of the substrate on (100) facet to play a role of independent seed crystal to form the frame of the cube by self-assembly as described in Figure 2(e). During this step, new layers come on the top to form cubic plates. Indeed, this model of growth of $CH_3NH_3PbBr_3$ (100) facet is proceed in layer-by-layer model. In general, to growth a macroscopic film, it needs a balance of surface energies of the substrate γ_B, the deposit γ_A, and the energy of the interface $\gamma*$ formed between the two (Figure 2(e)), which are controlled by the change in Gibbs free energy needed for the creation of the surface or interface [40, 41]. The layer by layer growth will be characteristic by the balance of energies that will support the increase of the area of the deposit (and the interface) over leaving an exposed substrate surface ($\gamma_A + \gamma* < \gamma_B$). The results of this growth will be a completion of one layer before the nucleation of subsequent layers occurs. This proposed model was confirmed by 3D fluorescence microscope and SEM observations, where the formation of layers is very clear in Figure 2(c) and support as well Chen's et al approach [29].

Since we have obtained the cubic phase for $CH_3NH_3PbBr_3$ perovskites in our experiments, the unit cell of simple cubic structure is considered for the calculations and the optimized crystal structure is shown in Figure 3(a). The room temperature crystal structure of $CH_3NH_3PbBr_3$ is cubic with Pm3m space group and we have obtained bulk lattice parameter of 5.92 Å after optimization, which agrees with experimentally reported value of 5.94 Å [42].

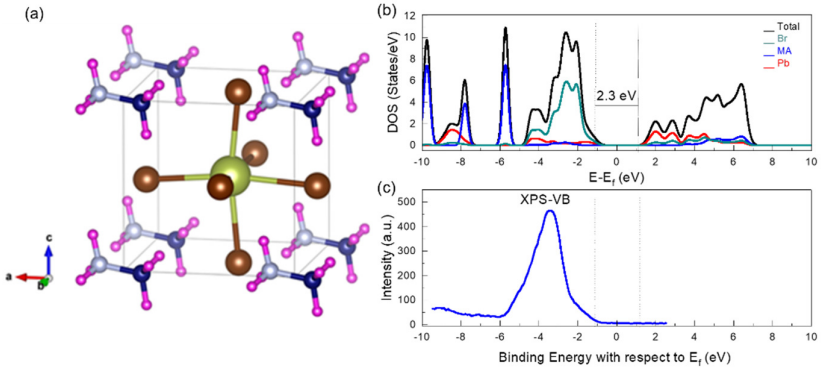

Fig. 3. The optimized structure of $CH_3NH_3PbBr_3$ unit cell. The atoms, respectively are, silver (Carbon), blue (Nitrogen), pink (Hydrogen), green (Pb) and brown (Br). Comparison of (b) calculated total and projected density of states (DOS) of $CH_3NH_3PbBr_3$ using GGA+U, (c) Experimental DOS measured by XPS VB.

The total density of states (DOS) as well as the projected density of states calculated for the individual atoms plotted using GGA+U is presented in Figure 3(b). We can see that main contribution close to the valence band maximum (VBM) comes from the halogen (Br) 4p states. The experimental DOS measured by XPS VB is presented in Figure 3(c). It can be seen that the features of XPS VB spectrum and theoretical DOS shows good agreement over wide energy range. The VBM also consists of smaller contribution from the Pb 6s and 6p orbitals. The $CH_3NH_3PbBr_3$ microstructures show a band gap of about 2.3 eV.

4 Conclusions

In summary, perovskite $CH_3NH_3PbBr_3$ microstructures were synthesized using a one-step solution self-assembly method. The morphology of these microstructures consists of a mixture of plates and cubes. We found that after crystallization of $CH_3NH_3PbBr_3$, hollow plates are formed on the substrate, and then a layer-by-layer growth model was used to the growth $CH_3NH_3PbBr_3$ cubes in (001) direction. The density of states calculated using DFT methods is in good agreement with XPS experimental results.

Acknowledgment

This work was supported by UAE University, under NSS Center Project No. 21R032 and UPAR- project No 31S306. S. Assa Aravindh gratefully acknowledge CSC -IT, Finland for computational resources and Academy of Finland (# 311934).

References

1. Jianxu, D., Xiaohua, C., Lin, J., Tianliang, Z., Ying, Z., Songjie, D.: Polarization-Dependent Optoelectronic Performances in Hybrid Halide Perovskite $MAPbX_3$ (X = Br, Cl) Single-Crystal Photodetectors. ACS Appl. Mater. Interfaces 10, 845-850 (2013).
2. Dong, J. Xu., Shi, J.J., Li, D.M., Luo, Y.H., Meng, Q.B., Chen, Q.: Suppressing Charge Recombination in ZnO-Nanorod-Based Perovskite Solar Cells with Atomic-Layer-Deposition TiO_2. Chin. Phys. Lett. 32, 078401 (2015).
3. Wong, A. B., Lai, M. L., Eaton, S. W., Yu, Y., Lin, E., Dou, L., Fu, A., Yang, P.D.: Growth and Anion Exchange Conversion of $CH_3NH_3PbX_3$ Nanorod Arrays for Light-Emitting Diodes. Nano Lett. (15) 5519 (2015).
4. Chao, L. M., Tai, T. Y., Chen, Y. Y., Lin, P.Y., Fu, Y.S.: Fabrication $CH_3NH_3PbI_3$/PVB Composite Fibers via Electrospening and Despositin. Materials 8, 5467-5478 (2015).
5. Tan, Z. K., Moghaddam, R.S., Lai, M. L., Docampo, P., Higler, R., Deschler, F., Price, M., Sadhanala, A., Pazos, L. M., Credgington, D.: Bright light-emitting diodes based on organometal halide perovskite. Nat. Nano. 9, 687 (2014).
6. Sutherland, B. R., Hoogland, S., Adachi, M.M., Wong, C.T.O., Sargent, E.H.: Conformal Organohalide Perovskites Enable Lasing on Spherical Resonators. ACS Nano 8, 10947 (2014).

7. Najar, A., Shafa, M., Anjum, D.: Synthesis, optical properties and residual strain effect of GaN nanowires generated via metal-assisted photochemical electroless etching. RSC Advances, 7 (35), 21697-21702 (2017).
8. Najar, A., Gerland, M., Jouiad, M.: Porosity-induced relaxation of strains in GaN layers studied by means of micro-indentation and optical spectroscopy. J. Appl. Phys. 111, 093513 (2012).
9. Najar, A., Omi, H., Tawara, T.: Scandium effect on the luminescence of Er-Sc silicates prepared from multi-nanolayer films. Nanoscale Research Letters 9, 1-6 (2014).
10. Najar, A., Ali Al-Jabr, A., Ben Slimane, A., Alsunaidi, M. A., Ng, T.K., Ooi, B.S., Sougrat, R., Anjum, D.H.: Effective antireflection properties of porous silicon nanowires for photovoltaic applications. IEEE Xplore (2013).
11. Ben Slimane, A., Najar, A., Ng, T.K., San-Román-Alerigi, D.P., Anjum, D., Ooi, B. S.: Surface States Effect on the Large Photoluminescence Redshift in GaN Nanostructures. Asia Communications and Photonics Conference, ATh3B. 3, (2013).
12. Najar, A., Omi, H., Tawara, T.: Effect of structure and composition on optical properties of Er-Sc silicates prepared from multi-nanolayer films. Optics Express, 23, 7021-7030 (2015).
13. Manser, J. S., Christians, J. A., Kamat, P.V.: Intriguing Optoelectronic Properties of Metal Halide Perovskites. Chemical Reviews 116, 12956−13008 (2016).
14. Snaith, H.V.: Perovskites: The Emergence of a New Era for Low-Cost, High-Efficiency Solar Cell. Physical Chemistry Letter 4, 3623−3630 (2013).
15. Saparov, B., Mitzi, D. B.: Organic−Inorganic Perovskites: Structural Versatility for Functional Materials Design. Chemical Reviews 116, 4558−4596 (2016).
16. Levy, M. R.: Crystal Structure and Defect Property Predictions in Ceramic Material. Imperial College of Science, Technology and Medicine (2005).
17. Yan, X., Wang, W., Yang, X., Yi, W., Wang, Y., Li, H., Gu, W., Sheng, C.: Origin of thermal instability of $CH_3NH_3PbI_3{-}xCl_x$ films for photovoltaic devices. Mater. Lett. 176, 114-117 (2016).
18. Tong, Y., Ehrat, F., Vanderlinden, W., Cardenas-Daw, C., Stolarczyk, J.K., Polavarapu, L., Urban, A.S.: Dilution-Induced Formation of Hybrid Perovskite Nanoplatelets. ACS Nano 10, 10936-10944 (2016).
19. Zhang, D., Eaton, S.W., Yu, Y., Dou, L., Yang, P.: Solution-Phase Synthesis of Caesium Lead Halide Perovskite Nanowires. J. Am. Chem. Soc. 137, 9230-9233 (2015).
20. Schmidt, L. C., Pertegás, A., González-Carrero, S., Malinkiewicz, O., Agouram, S., Espallargas, G.M., Bolink, H.J., Galian, R.E., Pérez-Prieto, J.: Nontemplate Synthesis of $CH_3NH_3PbBr_3$ Perovskite Nanoparticles. J. Am. Chem. Soc. 136, 850-853 (2014).
21. Dong, Q., Fang, Y., Shao, Y., Mulligan, P., Qiu, J., Cao, L., Huang, J.: Electron-hole diffusion lengths > 175 μm in solution-grown $CH_3NH_3PbI_3$ single crystals. Science 347, 967-970 (2015).
22. Ufuk, E., Pablo, S. F., Hyun, G. J., Keisuke, S., Yung, C. L., Mina, M., Kazu, S., Susumu, O., Kazunari, M., Hiroki, A. : Vapor Phase Selective Growth of Two-Dimensional Perovskite/WS_2 Heterostructures for Optoelectronic Applications. ACS Appl. Mater. Interfaces 11, 40503−40511 (2019).
23. Xing, J., Liu, X.F., Zhang, Q., Ha, S.T., Yuan, Y.W., Shen, C., Sum, T.C., Xiong, Q.: Vapor Phase Synthesis of Organometal Halide Perovskite Nanowires for Tuneable Room-Temperature Nanolasers. Nano Lett. 15, 4571-4577 (2015).
24. Liu, Y., Yang, Z., Cui, D., Ren, X., Sun, J., Liu, X., Zhang, J., Wei, Q., Fan, H., Yu, F., Zhang, X., Zhao, C., Liu, S. F.: Two-Inch-Sized Perovskite $CH_3NH_3PbX_3$ (X = Cl, Br, I) Crystals: Growth and Characterization. Adv. Mater. 27, 5176-5183 (2015).

25. Nayak, P. K., Moore, D. T., Wenger, B., Nayak, S., Haghighirad, A. A., Fineberg, A., Noel, N. K., Reid, O. G., Rumbles, G., Kukura, P., Vincent, K. A., Snaith, H. J.: Mechanism for rapid growth of organic-inorganic halide perovskite crystals. Nat. Commun. 7, 13303 (2016).
26. Rao, H. S., Li, W. G., Chen, B. X., Kuang, D. B., Su, C. Y.: In Situ Growth of 120 cm2 $CH_3NH_3PbBr_3$ Perovskite Crystal Film on FTO Glass for Narrowband-Photodetectors. Adv. Mater. 29, 1602639 (2017).
27. Shi, D., Adinolfi, V., Comin, R., Yuan, M., Alarousu, E., Buin, A., Chen, Y., Hoogland, S., Rothenberger, A., Katsiev, K., Losovyj, Y., Zhang, X., Dowben, P. A., Mohammed, O. F., Sargent, E. H., Bakr, O. M.: Low trap-state density and long carrier diffusion in organolead trihalide perovskite single crystals. Science 347, 519-522 (2015).
28. Hu, Q., Zhao, L., Wu, J., Gao, K., Luo, D., Jiang, Y., Zhang, Z., Zhu, C., Schaible, E., Hexemer, A., Wang, C., Liu, Y., Zhang, W., Gratzel, M., Liu, F., Russell, T. P., Zhu, R., Gong, Q.: In situ dynamic observations of perovskite crystallisation and microstructure evolution intermediated from $[PbI_6]$ 4- cage nanoparticles. Nat. Commun. 8, 15688 (2017).
29. Chen, F., Xu, C., Xu, Q., Zhu, Y., Zhu, Z., Liu, W., Dong, X., Qin, F., Shi, Z.: Structure Evolution of $CH_3NH_3PbBr_3$ Single Crystal Grown in N, N-dimethylformamide Solution, Cryst. Growth Des. 18, 3132-3137 (2018).
30. Liao, Q., Hu, K., Zhang, H., Wang, X., Yao, J., Fu, H.: Perovskite Microdisk Microlasers Self-Assembled from Solution. Adv. Mater. 27, 3405-10 (2015).
31. Zhang, Q., Ha, S.T., Liu, X., Sum, T.C., Xiong, Q.: Room-temperature near-infrared high-Q perovskite whispering-gallery planar nanolasers. Nano Lett. 14, 5995-6001(2014).
32. Kresse, G., Furthmüller, J.: Efficient iterative schemes for ab initio total-energy calculations using a plane-wave basis set. Phys. Rev. B. 54, 1116 (1996).
33. Qamhieh, N., Najar, A., Qamhieh, Z.N., Abdel Aziz, B., Mansour, A., Alghoul, I.: Synthesis and characterization of a perovskite film for solar cells applications. Optik, 171, 648-651 (2018).
34. Kresse, G., Hafner, J.: Ab initio molecular dynamics for liquid metals. Phys. Rev. B. 47, 558(R) (1993).
35. Blöchl, P. E.: Projector augmented-wave method. Phys. Rev. B. 50, 17953 (1994).
36. John, P. P., Kieron, B., Matthias, E.: Generalized Gradient Approximation Made Simple. Phys. Rev. Lett. 77, 3865 (1996).
37. Federico, B., Keith, T. B., Aron Mark, W. V. S.: Relativistic quasiparticle self-consistent electronic structure of hybrid halide perovskite photovoltaic absorbers. Phys. Rev. B. 89, 155204 (2014).
38. Eric, W., Luisa, S., Alex, Z.: Density functional theory + U modelling of polarons in organohalide lead perovskites. AIP Advances 6, 125037 (2016).
39. Peng, L., Dutta, A., Xie, R., Yang, W., Pradhan, N.: Dot–Wire–Platelet–Cube: step growth and structural transformations in $CsPbBr_3$ perovskite nanocrystals. ACS Energy Lett. 3, 2014–2020 (2018).
40. Venables, J. A.: Introduction to Surface and Thin Film. Processes Cambridge: Cambridge University Press (2000).
41. Burke, S. A., Topple, J. M., Gr¨utter, P.: Molecular dewetting on insulators. J. Phys.: Condens. Matter 21, 423101 (2009).
42. Noh, J. H., Im, S. H., Heo, J. H., Mandal, T. N., Seok, S. I.: Chemical management for colourful, efficient, and stable inorganic-organic hybrid nanostructured solar cells. Nano Lett. 13, 1764 (2013).